Onset of a Two-Dimensional Superconducting Phase in a Topological-Insulator–Normal-Metal $Bi_{1-x}Sb_x$/Pt Junction Fabricated by Ion-Beam Techniques

Dong-Xia Qu,[1,*] Nick E. Teslich,[1] Zurong Dai,[1] George F. Chapline,[1] Thomas Schenkel,[2] Sean R. Durham,[1] and Jonathan Dubois[1]

[1]*Lawrence Livermore National Laboratory, Livermore, California 94550, USA*
[2]*Lawrence Berkeley National Laboratory, Berkeley, California 94720, USA*

(Received 17 March 2018; revised manuscript received 1 May 2018; published 16 July 2018)

Inducing superconductivity in a topological insulator can lead to novel quantum effects. However, experimental approaches to turn a topological insulator into a superconductor are limited. Here, we report on superconductivity in topological insulator $Bi_{0.91}Sb_{0.09}$ induced via focused ion-beam deposition of a Pt thin film. The superconducting phase exhibits a Berezinski-Kosterlitz-Thouless transition, demonstrative of its two-dimensional character. From the in-plane upper critical field measurements, we estimate the superconducting thickness to be ~17 nm for a 5.5-μm-thick sample. Our results provide evidence that the interface superconductivity could originate from the surface states of $Bi_{0.91}Sb_{0.09}$.

DOI: 10.1103/PhysRevLett.121.037001

Recently, there has been huge interest in generating superconductivity on the surface of a topological insulator (TI) [1–5] because of its prospect to realize a new topological phase of matter, a topological superconductor [6–8]. Significant effort has been made to use the proximity effect [9–11] or to drive the bulk state of a TI into superconductivity [12–19]. Alternatively, interface superconductivity between a normal material and a TI has also been discovered [20–22]. It has been reported that the point contact between a normal metal and a Bi, Sb, or $Bi_{1-x}Sb_x$ alloy shows unusual properties that are ascribed to the presence of superconducting clusters [20]. This phenomenon was explained as a result of the difference in the contact potential, which generates an electric dipole layer at the junction and turns the semimetal, Bi and Sb, or semiconductor $Bi_{1-x}Sb_x$ into a superconductor [20,21]. However, the role played by the spin-polarized surface states that were recently discovered in $Bi_{1-x}Sb_x$ [23,24] for inducing the observed superconductivity has not been studied. Whereas for the Bi_2Te_3/FeTe heterostructure, interface superconductivity is hypothesized to arise from the FeTe layer—the presence of the surface states in Bi_2Te_3 increases the electron density of FeTe and turns FeTe into a superconductor [22]. It is well known that two-dimensional (2D) superconductors with strong spin-orbit coupling could exhibit unconventional pairing symmetries, such as a hybrid singlet-triplet pairing [25,26], Fulde-Ferrell-Larkin-Ovchinnikov pairing [27], and Ising pairing [28], because spin-orbit interaction locks the orientation of electron spin to its momentum. It is unclear whether the superconductivity in normal metal/$Bi_{1-x}Sb_x$ possesses a 2D or a three-dimensional property.

In this Letter, we demonstrate superconductivity at the Pt/$Bi_{0.91}Sb_{0.09}$ interface created by using a focused ion beam to directly write a Pt thin film onto a $Bi_{0.91}Sb_{0.09}$ single crystal. We find that superconductivity in samples with a $Bi_{0.91}Sb_{0.09}$ thickness < 6 μm has a 2D character evidenced by Berezinskii-Kosterlitz-Thouless (BKT) transition, the hallmark of a 2D superconductor [29–31]. From the $Bi_{0.91}Sb_{0.09}$-thickness-dependent upper critical field measurements, we provide the first experimental evidence showing that the 2D superconductivity occurs in the surface states of a TI.

The samples are prepared by depositing a thin Pt layer with a thickness of 100–200 nm on the (111) surface of a $Bi_{0.91}Sb_{0.09}$ single crystal [Fig. 1(a)]. The Pt films are grown in the middle of the channel by focused ion-beam (FIB) deposition with a Ga^+ ion-beam current of 93 pA, as shown in Fig. 1(b). We fixed Au wires onto the bulk samples using silver paste for four-point transport measurements. Table S1 in the Supplemental Material [32] summarizes the dimensions of $Bi_{0.91}Sb_{0.09}$ and Pt layers for six samples. The current is first injected into $Bi_{0.91}Sb_{0.09}$ and then flows through the $Bi_{0.91}Sb_{0.09}$/Pt interface. The voltage is measured along the junction area with a spacing of 40–140 μm. A Helium-3 cryostat is used for cooling the samples down to 0.35 K and a superconducting magnet is used for applying the magnetic field up to 6 T.

Figure 1(c) shows the high resolution transmission electron microscope (HRTEM) image of the clear interface between a FIB grown 200-nm-thick Pt film and the $Bi_{0.91}Sb_{0.09}$ substrate. The FIB deposited Pt film is amorphous at the interface, resulting in a slight lattice disorder in the 2-nm-thick Pt-intercalated $Bi_{0.91}Sb_{0.09}$ layer. The Pt-intercalation depth is estimated from the HRTEM imaging combined with the energy dispersive x-ray spectroscopy analysis (Fig. S1, Supplemental Material [32]). The surface roughness of the substrate is estimated to be less than ± 0.4 nm. There are no obvious dislocations away

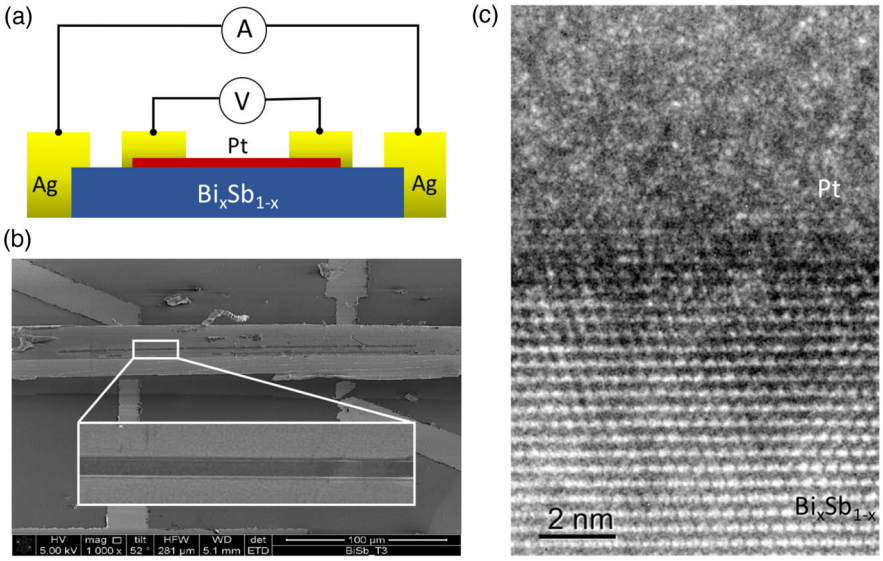

FIG. 1. (a) Sketch of the device structure and the measurement setup. (b) Scanning electron microscope image of the sample. (Inset) Enlarged top view of the region where the Pt layer is deposited. (c) High resolution transmission electron microscope image of a $Bi_{0.91}Sb_{0.09}$/Pt heterostructure.

from the interface into the bulk $Bi_{0.91}Sb_{0.09}$. For the $Bi_{0.91}Sb_{0.09}$ single crystals under study, the bulk electron and bulk hole carrier concentrations are comparable and highly compensated with a density $\sim 8.6 \times 10^{16}$ cm^{-3}, obtained from Hall and magnetoresistance measurements [24]. The Fermi level lies inside the bulk band gap and crosses the surface hole band with an average Fermi wave vector of $k_F = 0.033$ Å^{-1}.

The resistivity vs temperature $\rho_{xx}(T)$ profiles of Pt/$Bi_{0.91}Sb_{0.09}$ samples display a resistance drop at $T \sim 1.89$ K, whereas the pure $Bi_{0.91}Sb_{0.09}$ single crystal does not exhibit such a transition, as shown in Fig. 2(a). The critical temperature T_c, defined as $R(T_c) = 0.9 \times R(2.5\ \mathrm{K})$, does not vary significantly with the sample thickness for all three samples. We find that the resistance of the sample $TT4$ with $t = 5.5$ μm decreases by more than 97% from its normal state value, although it does not go to zero at the lowest temperature $T = 0.35$ K. We attribute the nonzero resistance to the fact that a portion of the voltage contact is anchored at the $Bi_{0.91}Sb_{0.09}$-Pt/$Bi_{0.91}Sb_{0.09}$ junction, where the normal material reservoir induces a static electric field penetrating into the superconductor [33]. As shown in the bottom inset of Fig. 2(a), the decreasing resistance corresponds to the standard theory for proximity-induced superconductivity $\delta R \propto T^{-1/2}$ [34] at $T < 0.8$ K. We also observe an additional steplike transition in the $\rho_{xx}(T)$ curves of two thick samples $TT1$ and $T3$ [arrows in the top inset of Fig. 2(a)]. We interpret this phenomenon as the existence of a Pt spreading layer deposited beyond the intended position via FIB. This is the so-called halo effect [35–38] (Fig. S6, Supplemental Material [32]). When we deposit a wide Pt layer covering the entire surface of $Bi_{0.91}Sb_{0.09}$, the steplike structure disappears (Fig. S5, Supplemental Material [32]).

Another interesting observation is the thickness-dependent $\rho_{xx}(T)$: the thinner samples are more likely to reach smaller remaining resistance. From magnetotransport measurements, we learn that the surface mobility is 6 times higher than the bulk mobility. With a Fermi velocity v_F of 1.1×10^5 m/s and a mean free path $l = 917$ nm for the surface state, we get the normal-metal coherence length ξ_N of 491 and 190 nm for surface and bulk states, respectively. When the sample thickness decreases, surface conduction becomes more dominant in thinner samples, which could give rise to a lower residue resistance because ξ_N for the surface state is more than 3 times larger than that of the bulk state. Moreover, since the surface of $Bi_{0.91}Sb_{0.09}$ becomes superconducting, bulk electrons have to travel a longer distance from current leads to voltage leads than surface electrons, leading to a larger voltage drop at the $Bi_{0.91}Sb_{0.09}$-Pt/$Bi_{0.91}Sb_{0.09}$ junction. We then expect thinner samples to display a lower resistance at $T < T_c$.

We now examine the details of the current-voltage (I-V) characteristics of the sample $TT4$ with $t = 5.5$ μm. It has been well known that, for 2D superconductors, the movement of thermally activated free vortex pairs should cause a nonlinear resistivity transition, the BKT transition [29–31]. At low temperature, the superconducting state consists of thermally excited bound vortex-antivortex pairs. Upon increasing temperature, the pairs break and induce a peculiar resistance change [39–41]. The vortex unbinding temperature, BKT temperature T_{BKT}, can be identified in the temperature dependence of the I-V relation, viz. $V \propto I^{\alpha(T)}$ with $\alpha(T_{\mathrm{BKT}}) = 3$ as the exponent best fitting of the curve. Our I-V curves are plotted on a log-log scale in Fig. 2(b). Above T_c, the I-V characteristics are exactly

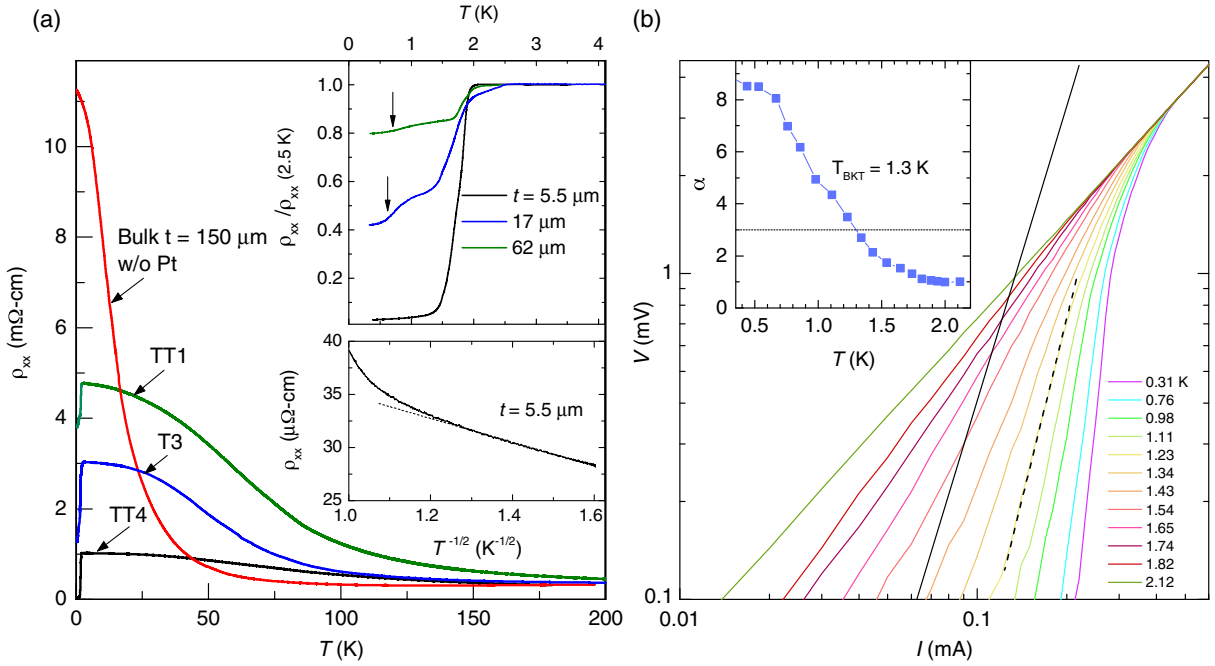

FIG. 2. (a) Resistivity ρ_{xx} vs temperature T profiles for four samples between 0.35 and 200 K. (Top inset) The normalized resistivity $\rho_{xx}/\rho_{xx}(2.5\ \mathrm{K})$ as a function of T for different samples. Arrows indicate the additional step transition below T_c. (Bottom inset) $\rho_{xx}(T)$ dependence of the $t = 5.5$-μm sample, plotted on a $T^{-1/2}$ scale. (b) Voltage V vs current I measurements of the 5.5-μm sample on a logarithmic scale. The short dashed line is the fit of the data in the transition. The long black line corresponds to $V \sim I^3$ dependence. (Inset) The extracted power-law exponent α as a function of T.

linear. As T falls below T_c, the curves are increasingly nonlinear. At $T = T_{\mathrm{BKT}}$, the I-V curve follows a power-law scaling of the form $V \propto I^3$. Below T_c, the current exponent increases, as commonly observed in 2D superconducting films. The extracted $\alpha(T)$ is shown in the inset. We observe $\alpha(T)$ approaches 3 at $T_{\mathrm{BKT}} = 1.3$ K, demonstrating that 2D superconducting states are developed at the interface of Pt and $Bi_{0.91}Sb_{0.09}$. Moreover, the $R(T)$ dependence also follows a BKT transition, consistent with our α-exponent analysis (Fig. S8, Supplemental Material [32]).

We next turn to the resistance measurement as a function of the magnetic field. Figure 3(a) shows the resistance R vs T curves in sample $TT4$ in a perpendicular magnetic field stepping from 0 to 1.4 T. The T-dependent critical fields, as defined by where $R(H_{c2}, T) = 0.9 \times R_N$ (R_N is the normal state resistance taken at 2.5 K), are plotted in Fig. 3(b) for samples $TT4$ and $TT1$. For both samples, under a perpendicular magnetic field (open squares) $H_{c2}^{\perp}$ shows a linear T dependence that follows $H_{c2}^{\perp} = [\phi_0/2\pi\xi(0)^2][1 - (T/T_c)]$, where ϕ_0 is the flux quanta and $\xi(0)$ is the Ginzburg-Landau coherence length at $T = 0$. A linear fit to the data close to T_c gives $\xi(0) = 15.8$ and 22.8 nm for $TT4$ and $TT1$, respectively.

The critical parallel field $H_{c2}^{\parallel}$, however, appears to be notably thickness dependent. For $TT4$ with $t = 5.5$ μm, $H_{c2}^{\parallel}$ vs T displays a square root dependence that is consistent with the behavior of a 2D superconductor $H_{c2}^{\parallel} = [\sqrt{3}\phi_0/\pi\xi(0)d_{\mathrm{sc}}][1 - (T/T_c)]^{1/2}$, where d_{sc} is the superconducting layer thickness [22,44,45]. The square root fit yields $d_{\mathrm{sc}} = 17.2$ nm for $TT4$, which is far less than the sample thickness 5.5 μm. For sample $TT1$, $H_{c2}^{\parallel}$ almost linearly depends on T, with a $H_{c2}^{\parallel}/H_{c2}^{\perp}$ ratio roughly 4.6. Fitting $H_{c2}^{\parallel}(T)$ in sample $TT1$ for $0.89 < T/T_c < 1$ [green curve, Fig. 3(b)] yields $d_{\mathrm{sc}} = 33.4$ nm, which is about twice as large as that of sample $TT4$. On the other hand, sample $BB2$ with $t = 23$ μm displays a stronger nonlinearity when compared with sample $TT1$, although its $H_{c2}^{\parallel}$ vs T profile deviates from the 2D behavior for $T/T_c < 0.64$ [orange curve, Fig. 3(b)]. By plotting the extracted d_{sc} for five different samples as a function of t in the inset of Fig. 3(b), we find that d_{sc} scales down as t decreases, suggesting 2D superconductivity becomes more dominant in thinner samples. Moreover, we observe that the magnitude of $H_{c2}^{\parallel}$ is significantly enhanced in thinner samples, as discussed in detail in Sec. IV of the Supplemental Material [32,46–49].

In a conventional superconductor, superconductivity can be destroyed in the presence of a large external magnetic field by the orbital and spin-Zeeman effects. In a 2D superconductor, however, the orbital effect is limited by the film thickness in a parallel magnetic field, leading to a square root T dependence of $H_{c2}^{\parallel}$. In contrast, in a 3D superconductor, $H_{c2}^{\parallel}$ scales linearly as a function of T in

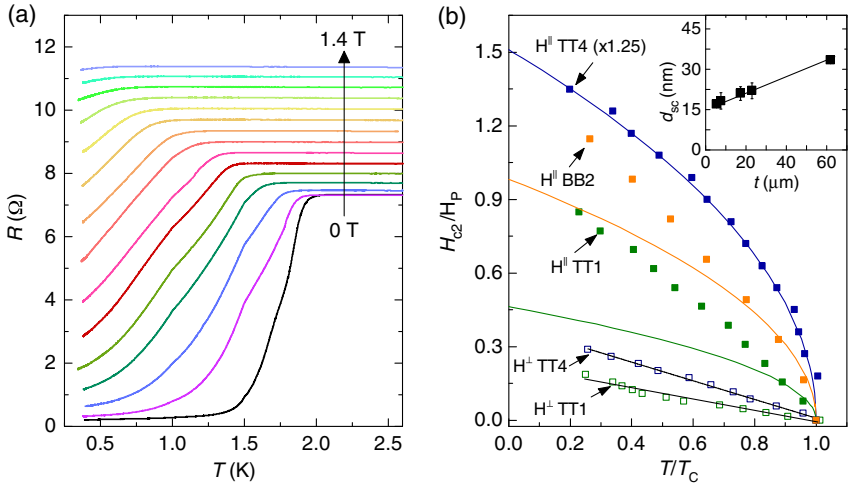

FIG. 3. (a) Resistance R of the 5.5-μm sample plotted as a function of T for magnetic fields applied perpendicular to the interface. (b) Temperature T/T_c dependence of the upper critical field H_{c2}/H_P under parallel (solid symbols) and perpendicular (open symbols) magnetic fields for samples $TT1$, $BB2$, and $TT4$. H_P is the Pauli paramagnetic limit [42,43]. The black lines are linear fits to $H_{c2}^{\perp} \propto 1 - T/T_c$. The green, orange, and blue curves are fits to $H_{c2}^{\parallel} \propto \sqrt{1 - T/T_c}$. $H_{c2}^{\parallel}$ for sample $TT4$ is magnified by 1.25 times for maximum clarity. (Inset) The extracted 2D superconductor thickness d_{sc} vs the $Bi_{0.91}Sb_{0.09}$ thickness t. The line is a guide to eyes.

both perpendicular and parallel field directions. In our case, when decreasing the thickness of $Bi_{0.91}Sb_{0.09}$, we find that $H_{c2}^{\parallel}$ vs T systematically transforms from a quasilinear to a square root dependence, quantitatively characterized by a decreasing 2D superconducting thickness d_{sc}. If the interface superconductivity only arises from the bulk states, d_{sc} should not vary with the sample thickness t, which, however, is contrary to the experimental observation [Fig. 3(b)]. Therefore, our results suggest that part of the 2D superconductivity originates from the surface states of a TI.

Figure 4(a) is a plot of differential resistance dV/dI vs I for different temperatures at zero magnetic field. Two broad peaks in dV/dI are observed at ± 0.35 mA, confirming that the junction is superconducting [as illustrated by the arrows in Fig. 4(a)]. In addition to the broad peaks, there are multiple nonperiodic sharp peaks, which could result from multiple superconducting islands caused by inhomogeneity of the Pt layer. A peak could occur each time the applied current exceeds the critical current of the two coupled islands [50,51]. In this case, the T-dependent 2D critical current is given by

$$I_{2D} \propto \Delta(T) \tanh[\Delta(T)/2k_B T], \tag{1}$$

where $\Delta(T)$ is the T-dependent superconducting energy gap and k_B is the Boltzmann constant [52]. With $T_c = 1.89$ K, we can achieve a very close fit by Eq. (1) to the T-dependent critical current (I_c^S), defined as the current at which the maximum sharp peak occurs for sample $TT4$ [red line, Fig. 4(b)]. In contrast, the T-dependent critical current

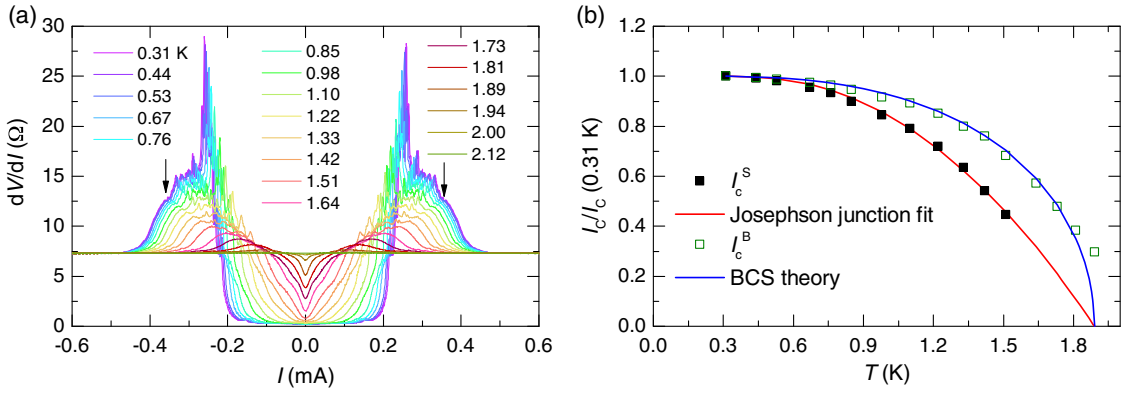

FIG. 4. (a) Differential resistance dV/dI as a function of current I. Arrows indicate the broad peak position. (b) The normalized critical current $I_c/I_c(0.31\ \mathrm{K})$ as a function of temperature T. I_c^S and I_c^B are the critical currents corresponding to the sharp and broad peaks in dV/dI vs I, respectively. The red and blue curves show the theoretical fits for I_c^S and I_c^B, respectively.

corresponding to the broad peak (I_c^B) is in good agreement with the BCS-like fit, typical for thin-film superconductors [53,54] [blue line, Fig. 4(b)]. Furthermore, these sharp peaks are absent in samples deposited with a large area Pt thin film and are suppressed by weak fields (Figs. S7 and S10, Supplemental Material [32,55,56]).

To explain the origin of the 2D superconductivity at the interface of a normal metal and a topological insulator requires more theoretical and experimental investigation. It was recently discovered that the Pt-3D Dirac semimetal Cd_3As_2 point contact also displays a superconducting phase [57,58]. Compared to previous work, in which superconductivity is created at a nanometer-scale junction, we demonstrate that a micrometer-scale superconductivity can be generated in the surface states of a TI via FIB deposition. This fabrication method might be used to induce an unconventional superconducting phase in a 3D topological Dirac semimetal as well. It is possible that the amorphous Pt layer changes the surface carrier concentration in a way to develop superconductivity. Moreover, the presence of surface states may provide excess carriers and further increase the electron density near the Pt layer, which helps to make the surface of $Bi_{0.91}Sb_{0.09}$ become superconducting. In future work, we can further investigate how the superconductivity varies with Sb doping to find out the role played by the topologically protected surface states in the induced 2D superconductivity, as $Bi_{1-x}Sb_x$ exhibits a topological phase transition at $x = 0.04$ [59].

In summary, we have demonstrated 2D superconductivity on the surface of a TI by fabricating a $Pt/Bi_{0.91}Sb_{0.09}$ heterojunction. Superconductivity involving topological Dirac surface states or spin-polarized 2D electron gas has recently been proposed as a platform to support Majorana fermions. It has been predicted that a Josephson junction formed with a 2D electron gas with strong spin-orbit coupling undergoes a topological phase transition in a parallel magnetic field [60]. Our studies reveal that surface superconductivity in a 3D TI is very different from that in an ordinary bulk material in terms of the thickness-dependent $R(T)$ and $H_{c2}^{\parallel}(T)$ properties. The identification of 2D Josephson junctions and the sample fabrication control reported here will provide an exciting starting point for future testing of fundamental physics predictions, such as the supercurrent rectifying effect and topological superconductivity.

We would like to thank Eric R. Schwegler, Yaniv J. Rosen, Sergey V. Pereverzev, and Liang Fu for helpful discussion. This work was performed under the auspices of the U.S. Department of Energy by Lawrence Livermore National Laboratory under Contract No. DE-AC52-07NA27344. The project was supported by the Laboratory Directed Research and Development (LDRD) programs of LLNL (15-LW-018 and 16-SI-004).

*qu2@llnl.gov

[1] C. L. Kane and E. J. Mele, Phys. Rev. Lett. **95**, 146802 (2005).
[2] L. Fu and C. L. Kane, Phys. Rev. B **76**, 045302 (2007).
[3] X.-L. Qi and S.-C. Zhang, Rev. Mod. Phys. **83**, 1057 (2011).
[4] M. Z. Hasan and C. L. Kane, Rev. Mod. Phys. **82**, 3045 (2010).
[5] D.-X. Qu, Y. S. Hor, J. Xiong, R. J. Cava, and N. P. Ong, Science **329**, 821 (2010).
[6] L. Fu and C. L. Kane, Phys. Rev. Lett. **100**, 096407 (2008).
[7] A. P. Schnyder, S. Ryu, A. Furusaki, and A. W. W. Ludwig, Phys. Rev. B **78**, 195125 (2008).
[8] M. Sato, Phys. Rev. B **81**, 220504(R) (2010).
[9] J. R. Williams, A. J. Bestwick, P. Gallagher, S. S. Hong, Y. Cui, A. S. Bleich, J. G. Analytis, I. R. Fisher, and D. Goldhaber-Gordon, Phys. Rev. Lett. **109**, 056803 (2012).
[10] M. Veldhorst, M. Snelder, M. Hoek, T. Gang, V. K. Guduru, X. L. Wang, U. Zeitler, W. G. van der Wiel, A. A. Golubov, H. Hilgenkamp, and A. Brinkman, Nat. Mater. **11**, 417 (2012).
[11] S.-Y. Xu, N. Alidoust, I. Belopolski, A. Richardella, C. Liu, M. Neupane, G. Bian, S.-H. Huang, R. Sankar, C. Fang, B. Dellabetta, W. Dai, Q. Li, M. J. Gilbert, F. Chou, N. Samarth, and M. Z. Hasan, Nat. Phys. **10**, 943 (2014).
[12] Y. S. Hor, A. J. Williams, J. G. Checkelsky, P. Roushan, J. Seo, Q. Xu, H. W. Zandbergen, A. Yazdani, N. P. Ong, and R. J. Cava, Phys. Rev. Lett. **104**, 057001 (2010).
[13] S. Sasaki, M. Kriener, K. Segawa, K. Yada, Y. Tanaka, M. Sato, and Y. Ando, Phys. Rev. Lett. **107**, 217001 (2011).
[14] Y. Qiu, K. Sanders, J. Dai, J. Medvedeva, W. Wu, P. Ghaemi, T. Vojta, and Y. S. Hor, arXiv:1512.03519.
[15] T. Asaba, B. J. Lawson, C. Tinsman, L. Chen, P. Corbae, G. Li, Y. Qiu, Y. S. Hor, L. Fu, and L. Li, Phys. Rev. X **7**, 011009 (2017).
[16] M. P. Smylie, K. Willa, H. Claus, A. Snezhko, I. Martin, W.-K. Kwok, Y. Qiu, Y. S. Hor, E. Bokari, P. Niraula, A. Kayani, V. Mishra, and U. Welp, Phys. Rev. B **96**, 115145 (2017).
[17] Z. Liu, X. Yao, J. Shao, M. Zuo, L. Pi, S. Tan, C. Zhang, and Y. Zhang, J. Am. Chem. Soc. **137**, 10512 (2015).
[18] Shruti, V. K. Maurya, P. Neha, P. Srivastava, and S. Patnaik, Phys. Rev. B **92**, 020506 (2015).
[19] G. Du, Y. Li, J. Schneeloch, R. D. Zhong, G. Gu, H. Yang, H. Lin, and H.-H. Wen, Sci. China Phys. Mech. Astron. **60**, 037411 (2017).
[20] L. Esaki and P. J. Stiles, Phys. Rev. Lett. **15**, 152 (1965).
[21] O. I. Shklyarevskii, A. M. Duif, A. G. M. Jansen, and P. Wyder, Phys. Rev. B **34**, 1956 (1986).
[22] Q. L. He, H. Liu, M. He, Y. H. Lai, H. He, G. Wang, K. T. Law, R. Lortz, J. Wang, and I. K. Sou, Nat. Commun. **5**, 4247 (2014).
[23] D. Hsieh, D. Qian, L. Wray, Y. Xia, Y. S. Hor, R. J. Cava, and M. Z. Hasan, Nature (London) **452**, 970 (2008).
[24] D.-X. Qu, S. K. Roberts, and G. F. Chapline, Phys. Rev. Lett. **111**, 176801 (2013).
[25] L. P. Gorkov and E. I. Rashba, Phys. Rev. Lett. **87**, 037004 (2001).
[26] T. Sekihara, R. Masutomi, and T. Okamoto, Phys. Rev. Lett. **111**, 057005 (2013).

[27] Y. Matsuda and H. Matsuda, J. Phys. Soc. Jpn. **76**, 051005 (2007).
[28] X. Xi, Z. Wang, W. Zhao, J.-H. Park, K. T. Law, H. Berger, L. Forró, J. Shan, and K. F. Mak, Nat. Phys. **12**, 139 (2016).
[29] N. Reyren, S. Thiel, A. D. Caviglia, L. Fitting Kourkoutis, G. Hammerl, C. Richter, C. W. Schneider, T. Kopp, A.-S. Rüetschi, D. Jaccard, M. Gabay, D. A. Muller, J.-M. Triscone, and J. Mannhart, Science **317**, 1196 (2007).
[30] J. M. Kosterlitz and D. J. Thouless, J. Phys. C **6**, 1181 (1973).
[31] B. I. Halperin and D. R. Nelson, J. Low Temp. Phys. **36**, 599 (1979).
[32] See Supplemental Material at http://link.aps.org/supplemental/10.1103/PhysRevLett.121.037001 for further details on the sample parameters, device fabrication, and transport characterization.
[33] G. R. Boogaard, A. H. Verbruggen, W. Belzig, and T. M. Klapwijk, Phys. Rev. B **69**, 220503(R) (2004).
[34] X. Jehl, M. Sanquer, R. Calemczuk, and D. Mailly, Nature (London) **405**, 50 (2000).
[35] R. C. Castillo, *Functional Nanostructures Fabricated by Focused Electron/Ion Beam Induced Deposition* (Springer International Publishing, New York, 2014), Chap. 5, p. 101.
[36] J. Wang, M. Singh, M. Tian, N. Kumar, B. Liu, C. Shi, J. K. Jain, N. Samarth, T. E. Mallouk, and M. H. W. Chan, Nat. Phys. **6**, 389 (2010).
[37] D. J. Resnick, J. C. Garland, J. T. Boyd, S. Shoemaker, and R. S. Newrock, Phys. Rev. Lett. **47**, 1542 (1981).
[38] S. Eley, S. Gopalakrishnan, P. M. Goldbart, and N. Mason, Nat. Phys. **8**, 59 (2012).
[39] M. R. Beasley, J. E. Mooij, and T. P. Orlando, Phys. Rev. Lett. **42**, 1165 (1979).
[40] A. F. Hebard and A. T. Fiory, Phys. Rev. Lett. **50**, 1603 (1983).
[41] O. Yuli, I. Asulin, O. Millo, D. Orgad, L. Iomin, and G. Koren, Phys. Rev. Lett. **101**, 057005 (2008).
[42] A. M. Clogston, Phys. Rev. Lett. **9**, 266 (1962).
[43] B. S. Chandraskhar, Appl. Phys. Lett. **1**, 7 (1962).
[44] M. Kim, Y. Kozuka, C. Bell, Y. Hikita, and H. Y. Hwang, Phys. Rev. B **86**, 085121 (2012).
[45] A. W. Tsen, B. Hunt, Y. D. Kim, Z. J. Yuan, S. Jia, R. J. Cava, J. Hone, P. Kim, C. R. Dean, and A. N. Pasupathy, Nat. Phys. **12**, 208 (2016).
[46] V. Barzykin and L. P. Gorkov, Phys. Rev. Lett. **89**, 227002 (2002).
[47] M. Tinkham, *Introduction to Superconductivity*, 2nd ed. (McGraw-Hill, New York, 1996).
[48] D. Rainer and G. Bergmann, J. Low Temp. Phys. **14**, 501 (1974).
[49] B. McCombe and G. Seidel, Phys. Rev. **155**, 633 (1967).
[50] Z. Wang, W. Shi, H. Xie, T. Zhang, N. Wang, Z. Tang, X. Zhang, R. Lortz, P. Sheng, I. Sheikin, and A. Demuer, Phys. Rev. B **81**, 174530 (2010).
[51] B. Bergk, A. P. Petrovic, Z. Wang, Y. Wang, D. Salloum, P. Gougeon, M. Potel, and R. Lortz, New J. Phys. **13**, 103018 (2011).
[52] V. Ambegaokar and A. Baratoff, Phys. Rev. Lett. **10**, 486 (1963); **11**, 104(E) (1963).
[53] E. F. Talantsev and J. L. Tallon, Nat. Commun. **6**, 7820 (2015).
[54] E. F. Talantsev, W. P. Crump, J. O. Island, Y. Xing, Y. Sun, J. Wang, and J. L. Tallon, 2D Mater. **4**, 025072 (2017).
[55] J. R. Gao, J. P. Heida, B. J. van Wees, T. M. Klapwijk, G. Borghs, and C. T. Foxon, Surf. Sci. **305**, 470 (1994).
[56] H. Y. Günel, N. Borgwardt, I. E. Batov, H. Hardtdegen, K. Sladek, G. Panaitov, D. Grützmacher, and Th. Schäpers, Nano Lett. **14**, 4977 (2014).
[57] L. Aggarwal, A. Gaurav, G. S. Thakur, Z. Haque, A. K. Ganguli, and G. Sheet, Nat. Mater. **15**, 32 (2016).
[58] H. Wang, H. Wang, H. Liu, H. Lu, W. Yang, S. Jia, X.-J. Liu, X. C. Xie, J. Wei, and J. Wang, Nat. Mater. **15**, 38 (2016).
[59] H. M. Benia, C. Strasser, K. Kern, and C. R. Ast, Phys. Rev. B **91**, 161406(R) (2015).
[60] F. Pientka, A. Keselman, E. Berg, A. Yacoby, A. Stern, and B. I. Halperin, Phys. Rev. X **7**, 021032 (2017).